Defence Technology 16 (2020) 275–282

Contents lists available at ScienceDirect

Defence Technology

journal homepage: www.keaipublishing.com/en/journals/defence-technology

A comparison of the ballistic behaviour of conventionally sintered and additively manufactured alumina

Gareth James Appleby-Thomas [a, *], Kevin Jaansalu [b], Amer Hameed [a], Jonathan Painter [a], James Shackel [a], Julie Rowley [a]

[a] Centre for Defence Engineering, Cranfield Defence and Security, Cranfield University, Shrivenham, Swindon, SN6 8LA, UK
[b] Department of Chemistry and Chemical Engineering, Royal Military College of Canada, PO Box 17000, Station Forces, Kingston, Ontario, K7K 7B4, Canada

ARTICLE INFO

Article history:
Received 6 May 2019
Received in revised form
28 May 2019
Accepted 19 June 2019
Available online 20 June 2019

Keywords:
Additive manufacture
Rapidly prototyped
Body armour
Ballistics
Ceramics

ABSTRACT

Production of ceramic armour solutions on-demand/in-theatre would have significant logistical and military advantages. However, even assuming that such technologies could be successfully deployed in the field, such near net-shape manufacturing technology is relatively immature compared to conventional sintering of ceramics. In this study, the ballistic performance of a series of additively manufactured (AM)/rapidly-prototyped (RP) alumina tiles of 97.2% of the density of Sintox FA™ were investigated using both forward- and reverse-ballistic experiments. These experiments, undertaken with compressed gas-guns, employed the depth-of-penetration technique and flash X-ray as primary diagnostics to interrogate both efficiency of penetration and projectile-target interaction, respectively. The RP alumina was found to exhibit useful ballistic properties, successfully defeating steel-cored (AP) 7.62 × 39 mm BXN rounds at velocities of up-to c.a. 850 m/s, while exhibiting comparable failure modes to conventionally sintered armour-grade Sintox FA™. However, where a <1% by vol. Cu dopant was introduced into the RP material failure modes changed dramatically with performance dropping below that of conventionally sintered alumina. Overall, the results from both sets of experiments were complimentary and clearly indicated the potential of such RP materials to play an active role in provision of real-world body armour solutions provided quality control of the RP material can be maintained.

1. Introduction

The high specific strength under impact of ceramics has led to their widespread adoption as armour materials against hardened rounds, both for personnel and for vehicles [1–7]. Such solutions are often composite in nature, with a compliant backing material employed to account for the inherently brittle nature of the hard ceramic facing (for additional detail in the body armour sphere, the reader is referred to a very complete recent review in Ref. [6] covering, in particular, ceramic strike-face materials, backing materials and cladding approaches). However, fitting a rigid armour solution to complex shaped structures (whether vehicles or even individuals, where significant variation in individual stature naturally occurs) is a crucial challenge. Further, such rigid systems – which may even need replacement in theatre (due to damage) – are inevitably relatively inefficient to transport due to a relatively high volume to density ratio. To this end, the ability to rapidly produce complex ceramic shapes in the field would be a significant advantage in terms of the continued deployment of ceramic armour to a wider range of applications.

High purity alumina (Al_2O_3) has been widely adopted as a body armour material, primarily due to its useful combination of good ballistic properties, low costs and familiarity with associated manufacturing routes [4]. Other ceramics such as silicon carbide (SiC) and boron carbide (B_4C) are stronger but are less widely employed due to both manufacturing and economic issues [3,4], although research into these materials is now very-much coming to the fore [6]. One of the main mechanisms governing ceramic armour response is that of overmatch of incident projectiles – leading to their erosion and subsequent defeat [8–10]. This process, known as dwell, only occurs below a certain threshold velocity,

* Corresponding author.
E-mail address: g.applebythomas@cranfield.ac.uk (G.J. Appleby-Thomas).
Peer review under responsibility of China Ordnance Society

https://doi.org/10.1016/j.dt.2019.06.020

while above this threshold velocity, if the defect population caused by the initial impact of projectile is sufficiently high, a transition to penetration can occur [11,12]. This threshold velocity is known as the dwell–penetration transition velocity. Essentially, dwell will continue as long as the defect population in the target is low enough that its strength is not overcome. Importantly, however, dwell will only occur if the target is held under compression – arrival of tensile releases of sufficient magnitude will promote armour failure. Such release waves can be generated at interfaces of lower impedance such as the rear surface or edges of an armour tile and, on arriving back at the point of impact, may lead to consequent material failure. This response – and the consequent importance of ceramic confinement – is highlighted by the radical difference in tensile and compressive strengths of ceramics (e.g. 300 and 2620 MPa respectively for 99.9% pure Al_2O_3 [13]).

There have been a large number of studies focused on understanding ceramic armour, with the aim of either defeating systems or improving their performance [4–20]. While these have identified numerous factors (including individual ceramic strength and target construction) which effect armour performance, the importance of overmatch means that control of wave propagation within the armour following impact is of particular importance to maximise efficiency.

Ceramic armour is typically manufactured via a pressure-sintering route, with differences (for example in temperature) effecting the final grain size and consequent material properties [4]. However, the ability to rapidly manufacture (3D print) ceramics is now slowly becoming more common-place. Several different routes exist; in particular, stereo lithography [21,22] (curing of photo-curable binder loaded ceramic pastes) and selective laser sintering [22,23] (involving laser sintering of green powder beds) are some of the more common approaches for ceramic materials, with other approaches including adapted forms of inkjet printing [24] and binder jetting [25].

In a typical study, ceramic armour failure modes under ballistic attack were interrogated via a combination of high-speed photography, flash X-ray and computational modelling [14]. Projectile erosion was shown to aid in conoid formation in the impacted ceramics – thereby maximising the extent of distribution of the projectiles impact energy onto the tougher backing plates. Interestingly, the thickness of such backing plates was also shown to be important – with thicker plates found to prevent premature failure of the ceramic, further highlighting the fact that ceramic armour solutions are composite in nature [15]. This is consistent with recent research for conventionally manufactured (pressure sintered) Al_2O_3 tiles which has linked ceramic performance with both the thickness and hardness of confining material [26–28]. In these experiments, performance was found to improve with confinement, indicating the importance of boundaries in ceramic response.

However, there is a relative paucity of information on the ballistic response of rapidly prototyped/3D printed ceramics. To this end, the authors have previously presented tentative evidence that the relative ballistic properties of a particular 3D printed and conventionally sintered alumina are broadly comparable [29]. In this study this previous work is extended to further highlight the potential application of such materials, manufactured commercially via a modified stereolithography process. In particular, potential limitations of 3D printed alumina are explored in greater depth – with a particular focus, via inclusion of new data, on the influence of dopants during manufacture. A combination of forward (depth of penetration) [26,30,31] and reverse [18,32,33] ballistics experiments were undertaken using both steel and WC-Co cored Armour Piercing (AP) ammunition with the aim of investigating not only 3D printed ceramic performance under ballistic attack, but also the underpinning material response (both projectile defeat and ceramic failure).

2. Materials

As detailed in Table 1, Sintox FA™ (95.0% Al_2O_3 – Morgan Advanced Materials) and a Rapid Prototyped (RP) ceramic (Technology Assessment and Transfer (T&AT) Inc., USA [21]), manufactured via a modified stereolithography process (which did not involve laser sintering), were investigated. In the latter case, a set of targets with <1% by volume Cu inclusions were also considered, with the Cu content determined in the final samples via EDX scanning and subsequent graphical analysis of metallographically prepared samples. Porosity was also measured using similar samples. In all cases micrographs were graphically analysed using the freely available software package 'ImageJ' [34]. Micrographs were turned into 8-bit images and made binary to highlight areas of porosity and/or pull-out as-required.

Scanning electron micrographs of the materials investigated are presented in Fig. 1. In order to determine whether any anisotropy was present (considered a potential issue for the RP material due to the manufacturing technique which incorporates an inherent directionality), perpendicular sections were considered in all cases. Grain boundaries are just discernible in the captured secondary electron images. Microstructurally, the RP materials were observed to be more refined and rounded; with the Sintox FA™ grains more angular in nature. In general, consistent with their conventionally sintered nature, the grains in the Sintox FA™ were similar in both the impact and perpendicular faces with an elongated form nominally 5 μm wide by 10 μm long. Whereas for the RP material, the ceramic grains appeared slightly more isotropic in form with a smaller size of around 2–3 μm (presumably the nominal size of the feedstock powder), with these grains agglomerated into groupings whose size was comparable to the Sintox grains. Interestingly, there was no significant difference in microstructure apparent between the perpendicular faces considered for the RP materials (Fig. 1(a)/(b) and Fig. 1 (e)/(f)) for the RP and RP(Cu) materials in terms of the impact face/side, respectively. This was reflected in a slightly higher hardness, despite the observed greater porosity, for both the RP (pure) and RP(Cu) (copper-doped) alumina cases (Table 1). The porosity values in Table 1 exclude the effect of pull-outs. In all three cases, based on optical analysis, overall porosity (voids) appeared relatively low at just a few percent – although their distribution is significantly coarser for the Sintox than for RP material. Further, once the relatively coarse regions of pull-out were excluded, it was evident that there was significantly lower porosity apparent in the pressure-sintered Sintox FA™ – as shown by the close packing, away from large pull-out based voids, of individual grains in Fig. 1(c) and (d). Interestingly, small copper contaminants can just be discerned in Fig. 1(e) and (f), with the (highlighted by red dashed circles) brighter inclusions – representing regions were charging was occurring around the embedded copper particles (confirmed as such via EDX analysis) – sitting along alumina grain boundaries. Of particular note was that, despite a higher hardness, there was a

Table 1
Key target material properties.

Ceramic	Rapidly Proto – typed (RP)		Sintox™ FA
	Pure	Cu-doped	
Density/(kg·m^{-3})	3729	3580	3737
% Porosity – voids only (face/side)	2.11/0.98	1.55/1.09	1.00/0.42
VH (10 kg) (face/side)	1121/1210	1162/1311	1,083, 1160
c_l/c_s (mm·μs^{-1}) – 5.0 MHz values	7.822/6.094	–	9.845/5.941
E/GPa	202	–	320

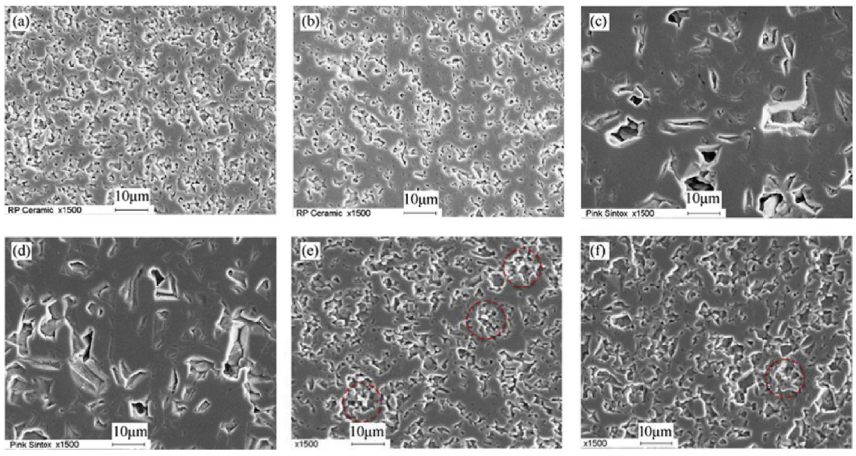

Fig. 1. Scanning electron micrographs showing rapid-prototyped and Sintox FA™ target ceramics(a) RP ceramic: impact face(b) RP ceramic: side(c) Sintox FA™: impact face(d) Sintox FA™: side(e) Cu-loaded RP ceramic: impact face(f) Cu-loaded RP ceramic: side; examples of Cu inclusions indicated by the bright regions highlighted in dashed red circles in (e) and (f).

notable difference in density of about 150 kg/m^3 (nominally 4%) between the RP(Cu) and the denser (pure) RP material. This appeared to be a real effect, although relatively small. Elastic properties in the form of longitudinal and shear sound speeds (c_l and c_s respectively) and Youngs modulus (E) were also determined using Panametrics ultrasonic transducers operating at 5.0 MHz for the pure RP and Sintox and are presented in Table 1. It was noted that longitudinal and shear sound speeds were significantly closer in the (pure) RP material as opposed to the pressure-sintered Sintox. Overall, it was apparent that differences in processing route and resultant microstructure led to the RP material exhibiting slightly greater porosity and consequent lower stiffness compared to the conventionally sintered Sintox FA™; however, in contrast, the more refined microstructure of the RP material led to a slightly higher hardness.

Differing hard and soft cored projectiles were used for forward and reverse-ballistics experiments, respectively, as shown in Fig. 2. While these projectiles had fundamentally different failure modes, they were selected to provide as much information as possible in a given experiment. In the forward configuration, WC-Co cored armour-piercing (AP) FFV 7.62 mm rounds provided enhanced penetration – and therefore fidelity in terms of subsequent depth-of-penetration measurements; whereas for reverse-ballistic experiments, the use of 7.62 mm steel-cored BXN Full Metal Jacket (FMJ) rounds encouraged dwell which was visible via flash X-ray.

3. Methodology

Both forward [26,30,31] and reverse [18,32,33] ballistic experiments were undertaken. Forward-ballistic experiments involved the use of a 30-mm smooth-bore single-stage compressed gas-gun to fire acetal-saboted WC-Co projectiles (Fig. 2(a)) into ceramic targets backed by a series of 100 mm^2 Al 6082 blocks, each of 25 mm thickness. Comparison of depths-of-penetration (DOP) into these backing plates allowed derivation of a metric known as 'mass efficiency' – E_m, to interrogate ballistic response. This approach, detailed later in Eq. (1) [3], allowed assessment of ballistic efficiency of the ceramic targets by comparing the depth-of-penetration of a projectile into a series of witness Al blocks with and with-out the presence of ceramic armour. For all forward-ballistic experiments the sabot was stripped from the projectiles just before impact, with velocity measured immediately prior to impact using a series of sequential light gates. This experimental

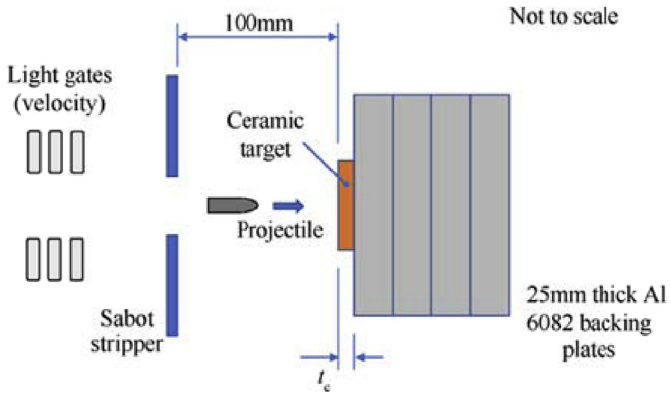

Fig. 3. Schematic illustration of forward-ballistic experimental arrangement.

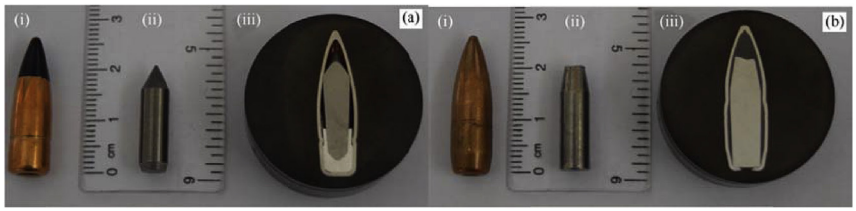

(a) WC-Co cored FFV round (b) steel-cored BXN Full Metal Jacket (FMJ) round

Fig. 2. 7.62 mm rounds employed for (a) forward and (b) reverse-ballistics experiments: (i) whole bullet; (ii) core only, and; (iii) cross-section. (a) WC-Co cored FFV round (b) steel-cored BXN Full Metal Jacket (FMJ) round.

arrangement is shown in Fig. 3.

For the reverse ballistic experiments, ceramic 'targets' were accelerated towards stationary 'projectiles' using a 50 mm bore single-stage gas-gun, with impacts monitored via four channels of Scandiflash XT-300 flash X-ray arranged radially around the impact point. This approach ensured that impact occurred at the desired point in the centre of the flash X-ray's focal area and, further, that the relatively small projectile did not yaw and that impacts were as normal to the target surface as possible. For these experiments the softer steel-cored BXN Full Metal Jacket (FMJ) projectiles were employed – as shown in Fig. 2(b) – as only projectile/target interaction was of interest. These rounds were the same as those employed in reverse ballistic experiments conducted within a previous study by Crouch et al. [33] focused on the interaction of steel-cored projectiles with Boron carbide ceramics. While alumina was employed here, this similarity provides a useful point of reference for the results presented later in this paper. This experimental arrangement is shown schematically in Fig. 4(a), with a picture of the target chamber illustrating the radial flash X-ray head arrangement presented in Fig. 4(b).

4. Results and discussion

Key experimental results for the forward and reverse ballistic experiments are presented in Table 2 and Table 3 respectively. While a limited number of samples were employed due to project constraints, target configurations were chosen to ensure that patterns in ballistic response (e.g. with sample thickness) would be apparent – ensuring that any general trends would be representative of real material response, even where experimental repetitions proved impractical. For the data in Table 2, mass efficiency (E_m) values were calculated based on Eq. (1) [3], using an average of baseline (Al backing only) DOP values (35.0 and 42.0 mm, both at an impact velocity of 848 m/s). This approach was considered reasonable in all cases as even for the relatively thin (c.a. 5 mm thick) ceramic tiles, backings were present – providing a 'semi-infinite' target configuration.

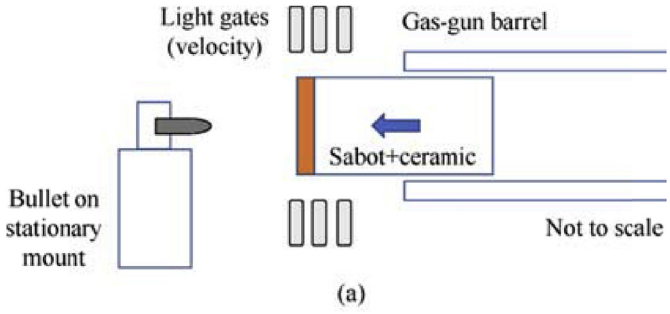

Fig. 4. Reverse ballistic experimental configuration: (a) schematic illustration; (b) external picture of target chamber with flash X-ray heads (silver tubes) arrayed around target position.

$$E_m = \frac{[\rho_{A1} \times P_\infty]}{[(t_c \times \rho_c) + (\rho_{A1} \times P_r)]} \quad (1)$$

Where: ρ_{Al} and ρ_c are the density of the Al backing and ceramic facing respectively; P_∞ is the DOP into the backing Al which results when no ceramic facing is present; t_c is the ceramic tile thickness, and; P_r is the residual DOP which results in the Al backing when the ceramic (armour) tile is present.

4.1. Forwards ballistics experiments

Based on Table 2, the variation of calculated mass efficiency with impacted ceramic thickness is illustrated in Fig. 5.

From Fig. 5 it is immediately apparent that for both RP and conventionally sintered alumina mass efficiency against the impacting AP FFV threat increases moving from 5 to 8 mm in ceramic thickness. Above this thickness, there is tentative evidence that the performance of the RP material is plateauing or even reducing. While this might suggest that the material's ballistic limit has been reached, there is insufficient data to draw any significant conclusions. It is notable, however, that at thicknesses of both 5 and 8 mm the RP material consistently shows a lower overall mass efficiency than the corresponding thickness Sintox FA™ targets. This reduction in efficiency is attributed to the slightly greater porosity of the RP material (see Table 1) which results in a reduction in material strength under loading. This is despite a slight increase in RP material hardness over the conventionally sintered alumina. In a similar vein, it is also interesting to note the significantly lower mass efficiency of the Cu-doped sample considered as opposed to the corresponding (8-mm thick) pure RP sample. Essentially, a reduction in E_m of nominally 43% occurs (relative to the Sintox) due to the small Cu addition as-opposed to just 18% moving from Sintox to pure RP material. This suggests, for the materials considered here, a significant relationship between RP ceramic purity and ballistic performance.

4.2. Reverse ballistics experiments

The variation of recovered core length with ceramic properties for the two nominal velocity regimes investigated is presented in Fig. 4 (with data taken from Table 3). In addition, selected results from previous similar reverse ballistics experiments conducted by Crouch et al. [33] are included for the purpose of comparison. These experiments involved identical projectiles to those employed here, but instead of alumina, Boron carbide ceramic discs of varying thicknesses were employed. Data is only included for tests which employed planar discs with no cladding (defined as 'support condition A' in Ref. [33]).

Fig. 6 clearly shows that increased ceramic thickness leads to greater core erosion – e.g. enhanced projectile defeat. This is relatively unsurprising as a greater ceramic thickness will allow for a corresponding increase in projectile/target (armour) interaction time. This is the gap between generation of waves at the moment of impact in the target and their arrival back at the point of impact (as tensile waves) following reflection at the ceramics rear face (e.g. a free surface). The conventionally sintered alumina and pure RP material are observed to exhibit broadly comparable behaviours, with nominally similar resultant projectile erosion for a given thickness of tile. Interestingly, the Boron carbide data [33] – despite lower impact velocities – appears to overlap with the general

Table 2
Forward-ballistics experimental results.

Exp. no.	Ceramic	Thickness/mm	E_m	Dimensions/mm	$V_{impact}/(m \cdot s^{-1})$	DOP/mm
1	Sintox FA™	5.00	1.8	45	856	14.3
2	Sintox FA™	8.00	2.5	50 × 50	848	4.4
3	Sintox FA™	8.10	2.4	100 × 100	833	4.8
4	RP	5.40	0.7	70	868	45.0
5	RP	8.20	2.0	70	856	7.9
6	RP	10.20	2.0	70	856	5.6
7	RP(Cu)	8.09	1.4	70	848	17.5

Table 3
Reverse-ballistics experimental results [Sintox FA/RP ceramic Ø 45/48 mm respectively].

Exp. no.	Ceramic	Thickness/mm	$V_{impact}/(m \cdot s^{-1})$	Recovered core length/mm
8	Sintox FA™	5.0	770	12.5
9	Sintox FA™	5.0	798	11.2
10	Sintox FA™	5.1	853	10.7
11	Sintox FA™	9.1	872	7.4
12	RP	5.3	765	13.1
13	RP	8.2	750	9.2
14	RP	10.2	750	7.0
15	RP	5.4	852	13.3
16	RP	8.3	852	9.7
17	RP	10.2	872	10.0
18	RP(Cu)	5.1	797	17.7
19	RP(Cu)	10.0	700	10.0
20	RP(Cu)	5.0	850	18.1
21	RP(Cu)	8.0	849	16.4
22	RP(Cu)	8.1	850	8.4

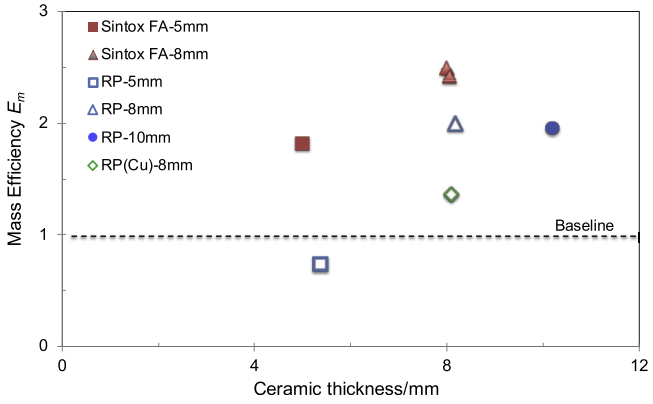

Fig. 5. Variation of calculated mass efficiency with impacted ceramic thickness.

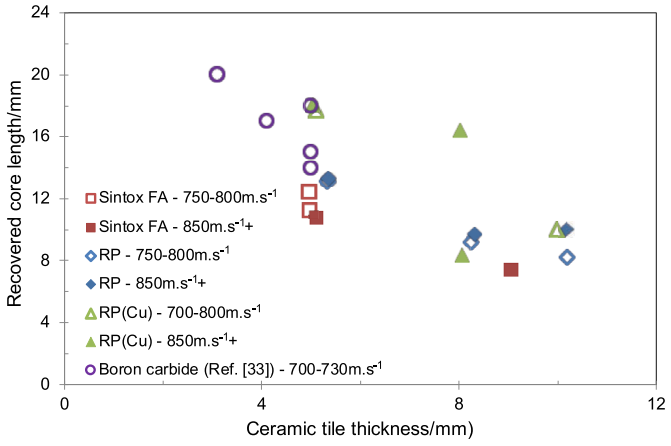

Fig. 6. Variation of recovered core length with impacted ceramic thickness including data from Ref. [33] for Boron carbide.

trends observed; this is likely due to the higher strength of the Boron carbide leading to greater erosion at a given impact velocity than for the alumina tiles considered here. More generally, the consistent trends for the conventionally sintered alumina, pure RP materials and Boron carbide apparent in Fig. 6 suggest that the pure RP alumina is behaving under impact in a comparable manner (exhibiting similar failure mechanisms) to other real-world armour ceramics despite differences in strength, increasing the applicability of the findings here. Overall in Fig. 6 projectile erosion appears to increase linearly with ceramic thickness. For the Sintox, it is notable that erosion is in all cases greater than that of comparable-thickness RP material. Further, for the 5 mm thick tiles, a higher velocity leads to greater erosion; this is likely due to the enhanced pressure induced on impact in the impacted ceramic/the corresponding increased apparent material strength (e.g. a steric or strain-rate hardening effect [30]).

With the RP material a similar trend is again apparent, with increased tile thickness linearly scaling with enhanced projectile erosion. However, it is interesting to note that for 5 and 8 mm thick tiles the degree of erosion appears to be relatively consistent and thus independent of impact velocity. While tentative, given the small number of data points, this may suggest that elements of the rapidly prototyped material structure (e.g. porosity) are such that the steric-effect observed in the conventionally sintered Sintox is no longer apparent in these velocity regimes. This is backed by the fact that divergence between the lower and higher velocity RP data points increases with increasing ceramic target thickness. In particular, at a thickness of 10 mm the highest velocity impact leads to lower overall projectile erosion (from Table 3, projectile erosion for the RP material was 10.0 and 13.0 mm for impacts at 750 and 872 m/s respectively, based on a nominal initial BXN steel core length of 20 mm as shown in Fig. 2(b)).

When the copper-doped alumina – RP(Cu) – is considered in Fig. 6, however, a more complex response appears to occur. While a general increase in ability to erode the incident projectiles with increasing ceramic thickness is again apparent, in the majority of cases the RP(Cu) ceramic performs less effectively (e.g. less projectile erosion results) than the corresponding thicknesses of both (pure) RP and conventionally sintered alumina. This is accompanied by a significant increase in variability of the resultant recorded core lengths at higher impact velocities. On this front it is notable that unlike the RP material, at a thickness of 5 mm there is no discernible difference in core erosion between the lower and higher impact velocity cases for the RP(Cu) alumina. This lack of a velocity (and therefore pressure) dependant effect where the ceramic otherwise appears to be behaving in a consistent manner appears to suggest that the presence of the RP(Cu) is modifying the material failure mode. In particular, the observed variability in the 8 mm thick RP(Cu) ceramic 850 m/s + results in Fig. 6 may suggest that the copper-doped material has a lower transition threshold (from dwell to penetration for a given projectile). This supposition was backed by the captured flash X-rays gained during the reverse-ballistics experiments.

Typical flash X-rays for the four different reverse-ballistics cases detailed in Table 3 are shown in Fig. 7(a) to Fig. 7 (d) covering experiments 10 (Sintox – 3 frames only), 12 (RP alumina), 19 and 20 (both Cu-loaded RP alumina), respectively. The general response shows flow of the jacketed rounds at/beneath the initial impact surface. This is consistent with behaviour observed by Crouch et al. [33] for Boron carbide ceramics, further reinforcing the suggestion that results presented here represent underlying mechanisms and are applicable to more than just alumina. From Fig. 7, an apparent marked difference in dwell – and subsequent penetration – mechanism between the 5 mm thick Sintox and RP(Cu) samples in Fig. 7(a) and (d), respectively, is of particular note. In terms of interpretation, it is also worth noting that for these reverse ballistic experiments, ceramic response will be a function of release arrival. Consequently, even if possible to neglect the rear interface by assuming that material around the point of impact is retained under compression by the impactor, releases from the outer edge of the impactor will have arrived as soon as 4.6 μs after impact (this is based on a nominal impactor diameter of 45 mm and elastic sound speed of 9.845 mm/μs – Tables 1 and 3, respectively). However, despite this limitation, these experiments still provide a direct indication of the ceramic/projectile interaction at impact and the nature of subsequent failure modes. The validity of this approach is reinforced by the fact that – as shown in Fig. 6 – even thinner ceramics have been employed in previous similar studies [33], with useful results still drawn out.

Fig. 7 presents flash X-rays detailing all three types of ceramic – namely Sintox, RP and RP(Cu) – investigated here. Considering each type of ceramic in turn:

Sintox FA^{TM}: Fig. 7(a) illustrates the typical response of an armour ceramic [27–33]; the projectile is observed to deform on impact and by 7 μs after the initial frame material is flowing radially away from and just beneath the impact surface (e.g. at the compressed surface of the ceramic) – as shown by the red arrows/dashed line. This behaviour, known as dwell/surface defeat [8–12] occurs while the ceramic is under compression (under which conditions its strength exceeds that of the core, overmatching/eroding it). Dwell only ceases either once the compressive loading is released via rarefaction's from the ceramic edges or rear-most face (free surface), or if the defect accumulation in the ceramic caused by the projectile impact is such that its strength is overcome [12]. In this manner, keeping the ceramic confined (in compression) maximises the opportunity for dwell.

RP Ceramic: Broadly similar behaviour to that for the Sintox FA™ in Fig. 7(a) is apparent for the pure RP material in Fig. 7(b). At 10 μs after the initial frame material flow (indicated by a red arrow) is apparent. Comparing the ceramic response at 20 μs to that for the Sintox FA™ target at 17 μs in Fig. 7(a), the extent of projectile erosion as the core reaches the rear surface of the ceramic appears directly comparable, albeit with penetration taking slightly longer – something attributed here to the slightly lower impact velocity in the RP material case. Overall, this response appears to confirm the potential of 3D printed material to respond in a similar manner to conventionally sintered ceramics. Finally, at 30 μs in Fig. 7(b) bulging of the rear face of the ceramic is apparent – however, interestingly, this is slightly asymmetric, with its extent likely linked to the degree of core disruption.

RP Ceramic – copper-doped: Similar behaviour to that for the Sintox and (pure) RP material in Fig. 7(a) and (b), respectively, is apparent for the thicker RP material detailed in Fig. 7(c), with surface defeat apparent at 10 μs (indicated by the red line/arrows). Although it is interesting to note that failure (via flexure) appears to have occurred at the rear of the ceramic at 35 μs – a time period consistent with that for failure in the thinner 5 mm case in Fig. 7(b). This is consistent with the data from Fig. 6 which suggested that under the impact conditions in question the RP material was potentially reaching a nominal limiting thickness in terms of

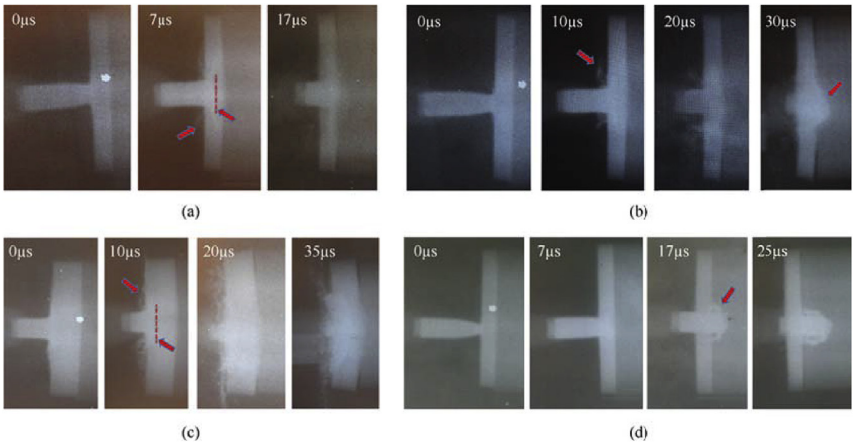

Fig. 7. Flash X-ray radiographs illustrating the interaction of 7.62-mm steel-cored rounds impacted by ceramic-faced flyer plates. (a) Experiment 10: 5.1-mm thick Sintox FATM at 853 m/s (three frames only as channel 4 miss-fired) (b) Experiment 12: 5.3-mm thick RP alumina at 765 m/s(c) Experiment 19: 10.0-mm thick RP(Cu) alumina at 700 m/s(d) Experiment 20: 5.0-mm thick RP(Cu) RP alumina at 850 m/s.

performance at around 8–10 mm. A substantially different response occurs with the RP(Cu) alumina in Fig. 7(d), however. In this case at the elevated impact velocity in question (850 m/s as opposed to 700 m/s in Fig. 7(c)), only very limited projectile flow occurs on impact. Instead, by 7 μs after the initial frame the core has passed relatively un-damaged through the impacting ceramic flyer – essentially a 'plugging'-like failure mode. While there is evidence of some core erosion in subsequent flash X-rays, this was measured post-shot to be just 1.9 mm (experiment 20, Table 3). This compares to 6.7 and 9.3 mm in the comparable 5 mm thick (pure) RP and conventionally sintered (Sintox) alumina experiments (experiments 15 and 10, Table 3), respectively. This difference in ballistic response of the RP(Cu) as opposed to the RP material may be linked to the observed enhanced hardness which resulted from the presence of the copper dopant (Table 1), with the copper particles dispersed at the alumina grain boundaries, shown in Fig. 1(e) and (f), potentially acting as initiation sites for a more brittle failure mode. Overall, the difference in response (an 80% reduction in projectile erosion compared to the conventional alumina as opposed to a drop-off of 28% for the pure RP ceramic case) clearly illustrates the significant effect of even the observed relatively small <1 wt% copper-doping, emphasising the importance of quality control.

5. Conclusions

A combination of forward- and reverse-ballistics experiments have provided insight into the potential application of RP ceramics to body armour applications. Both conventionally sintered and RP materials exhibited broadly similar microstructures and material properties, with observed differences in (surface) porosity and hardness attributed to a slightly more refined microstructure in the RP case. Experimental results suggest that where care is taken in quality control during manufacture the RP material can produce a slightly less effective, but overall broadly comparable, ballistic response against hardened/AP threats as opposed to conventionally sintered alumina (Sintox). Further, comparison to data from the literature [33] suggested that the behaviour of the pure RP material was broadly consistent with other armour ceramics, suggesting similar underlying projectile defeat/ceramic failure mechanisms. Overall, this is a useful result given the relatively limited body of existing work on armour-relevant RP ceramic materials in the literature, suggesting a potential future application for the RP alumina considered here.

Interestingly, however, forwards ballistics data suggested that the RP material has a slightly lower ballistic limit than the Sintox FA™ (evidenced by an apparent plateau in calculated mass efficiency as tile thickness increased from 8 to 10 mm). This suggests that there are some subtle differences in material response under impact linked to the manufacturing route/resultant material microstructure. This finding was reinforced by comparison of recovered projectile cores post-shot, as well as flash X-ray images captured during reverse ballistic experiments. The flash X-ray images clearly indicated that projectile defeat involves a similar mechanism (namely that of dwell) for both the RP and conventionally sintered ceramics. While a notable change in failure mode was observed where Cu additions were present, such behaviour was not apparent when un-doped/pure RP targets were considered.

Overall, while the experimental work presented in this study is based on a limited number of experiments, the presence of clear trends in data provided reassurance that key conclusions were valid. The results presented clearly highlight the importance of quality control if RP ceramics are to be deployed in critical areas such as body armour. Despite this, and while not considering the practicality of deploying 3D printers in-theatre (something beyond the scope of this study), the findings of this paper clearly illustrate the potential for use of such 3D printed materials in armour applications in the future.

Acknowledgements

The authors are grateful to Andrew Roberts of Cranfield University for aid in the experimental work presented in this paper. In addition, the authors would like to acknowledge the data presented herein is taken from a recent Explosives Ordnance Engineering MSc project conducted by one of the current authors at Cranfield University's Shirvenham Campus, Miss Julie Rowley. Finally, the authors would like to dedicate this work to their colleague, Dr Michael Gibson, who sadly passed away while the paper was being written.

References

[1] Yanagida H, Koumoto K, Miyayama M. The chemistry of ceramics. West Sussex, UK: John Wiley & Sons; 1996. p. 1–2.
[2] Scott RA. Textiles for protection. Cambridge, UK: Woodhead Publishing; 2005. p. 530–2.
[3] Hazell PJ. Ceramic armour: design and defeat mechanisms. Canberra, Australia: Argos Press; 2006.
[4] Medvedovski E. Ballistic performance of armour ceramics: influence of design and structure. Part 1. Ceram Int 2010;36(2). 103-2, 115, https://doi.org/10.1016/j.ceramint.2010.05.021.
[5] Medvedovski E. Ballistic performance of armour ceramics: influence of design and structure. Part 2. Ceram Int 2010;36(2). 117-2, 127, https://doi.org/10.1016/j.ceramint.2010.05.022.
[6] Crouch IG. Body armour – new materials, new systems. Def Technol. https://doi.org/10.1016/j.dt.2019.02.002.
[7] Hazell PJ, Fellows NA, Hetherington JG. A note on the behind armour effects from perforated alumina/aluminium targets. Int J Impact Eng 1998;21(7):589–95. https://doi.org/10.1016/S0734-743X(98)00014-1.
[8] Hauver GE, Rapacki EJ, Netherwood PH, Benck RF. Interface defeat of long-rod projectiles by ceramic armour. Army Research Laboratory Report; 2005.
[9] Normandia MJ, LaSalvia JC, Gooch JrJr, McCauley JW. Protecting the future force: ceramics research leads to improved armor performance. AMPTIAC Q 2004;8:21–7.
[10] Lundberg P. Interface defeat and penetration: two modes of interaction between metallic projectiles and ceramic targets. PhD Thesis. Sweden: Uppsala University; 2004.
[11] Holmquist TJ, Anderson JrJr, Behner T, Orphal DL. Mechanics of dwell and post-dwell penetration. Adv Appl Ceram 2010;109(8):467–79. https://doi.org/10.1179/174367509X12535211569512.
[12] Aydelotte B, Schuster B. Impact and penetration of SiC: the role of rod strength in the transition from dwell to penetration. Procedia Eng 2015;103:19–26. https://doi.org/10.1016/j.proeng.2015.04.004.
[13] Materials properties charts, Ceramic Industry, accessed 3 May, 2019, https://www.ceramicindustry.com/ext/resources/pdfs/2013-CCD-Material-Charts.pdf.
[14] Wilkins ML. Mechanics of penetration and perforation. Int J Eng Sci 1978;16:793–807. https://doi.org/10.1016/0020-7225(78)90066-6.
[15] Hazell PJ. Measuring the strength of brittle materials by depth-of-penetration testing. Adv Appl Ceram 2010;109:504–10. https://doi.org/10.1179/174367610X12804792635387.
[16] Franzen RR, Orphal DL, Anderson JrJr. The influence of experimental design on depth of penetration (DOP) test results and derived ballistic efficiencies. Int J Impact Eng 1997;19:727–37. https://doi.org/10.1016/S0734-743X(97)00010-9.
[17] Woodward RL, Baxter BJ. Ballistic evaluation of ceramics: influence of test conditions. Int J Impact Eng 1994;15:119–24. https://doi.org/10.1016/S0734-743X(05)80024-7.
[18] Hazell PJ, Appleby-Thomas GJ, Philbey D, Tolman W. The effect of gilding jacket material on the penetration mechanics of a 7.62 mm armour-piercing projectile. Int J Impact Eng 2013;54:11–8. https://doi.org/10.1016/j.ijimpeng.2012.10.013.
[19] Madhu V, Ramanjaneyulu K, Bhat TB, Gupta NK. An experimental study of penetration resistance of ceramic armour subjected to projectile impact. Int J Impact Eng 2005;32:337–50. https://doi.org/10.1016/j.ijimpeng.2005.03.004.
[20] Walley SM. Historical review of high strain rate and shock properties of ceramics relevant to their application in armour. Adv Appl Ceram 2010;109(8):446–66. https://doi.org/10.1179/174367609X422180.
[21] Technology assessment and transfer, Inc.; Ceramic 3D Printing (3D-CSL). http://techassess.com/technologies/ceramic-3d-printing-3d-csl. [Accessed 3 May 2019].
[22] Kruth J-P, Leu MC, Nakagawa T. Progress in additive manufacturing and rapid prototyping. Ann CIRP 1998;47(2):525–40. 1998, https://doi.org/10.1016/S0007-8506(07)63240-5.
[23] Bertrand Ph, Bayle F, Combe C, Goeuriot P, Smurov I. Ceramic components

manufactured by selective laser sintering. Appl Surf Sci 2007;254:989–92. https://doi.org/10.1016/j.apsusc.2007.08.085.
[24] Maleksaeedi S, Eng H, Wiria FE, Ha TMH, He Z. Property enhancement of 3D-printed alumina ceramics using vacuum infiltration. J Mater Process Technol 2014;214(7):301–6. 1, https://doi.org/10.1016/j.jmatprotec.2014.01.019.
[25] Gonzalez JA, Mireles J, Lin Y, Wicker RB. Characterization of ceramic components fabricated using binder jetting additive manufacturing technology. Ceram Int 2016;42(9):559–64. 10, https://doi.org/10.1016/j.ceramint.2016.03.079.
[26] Espinosa HD, Brar NS, Yuan G, Xu Y, Arrieta V. Enhanced ballistic performance of confined multi-layered ceramic targets against long rod penetrators through interface defeat. Int J of Solids and Struct 2000;37(36):893–913. 4, https://doi.org/10.1016/S0020-7683(99)00196-1.
[27] Anderson JrJr, Royal-Timmons SA. Ballistic performance of confined 99.5% Al_2O_3 ceramic tiles. Int J Impact Eng 1997;19(8):703–13. https://doi.org/10.1016/S0734-743X(97)00006-7.
[28] Tan ZH, Han X, Zhang W, Luo SH. An investigation on failure mechanisms of ceramic/metal armour subjected to the impact of tungsten projectile. Int J Impact Eng 2010;37(12):162–9. 1, https://doi.org/10.1016/j.ijimpeng.2010.07.004.
[29] Appleby-Thomas G, Hameed A, Wood D, Rowley J, Jaansalu K. On the ballistic response of rapidly-prototyped alumina. In: Proc. – 29th Int. Symp. on Ballistics, Vol. 2; 2016. p. 296–306. 2.
[30] Appleby-Thomas GJ, Wood DC, Hameed A, Painter J, Fitzmaurice B. On the effects of powder morphology on the post-comminution ballistic strength of ceramics. Int J Impact Eng 2017;100:46–55. https://doi.org/10.1016/j.ijimpeng.2016.10.008.
[31] Hazell PJ, Appleby-Thomas GJ, Toone S. Ballistic compaction of a confined ceramic powder by a non-deforming projectile: experiments and simulation. Mater Des 2014;56:943–52. https://doi.org/10.1016/j.matdes.2013.12.042.
[32] Hazell PJ. Armour: materials, theory, and design. Florida, USA: CRC Press; 2015.
[33] Crouch IG, Appleby-Thomas G, Hazell PJ. A study on the penetration behaviour of mild-steel-cored ammunition against boron carbide armours. Int J Impact Eng 2015;80:203–11. https://doi.org/10.1016/j.ijimpeng.2015.03.002.
[34] Image processing and analysis in Java (ImageJ). https://imagej.nih.gov/ij/index.html. [Accessed 13 December 2018].

A comparison of the ballistic behaviour of conventionally sintered and additively manufactured alumina

Appleby-Thomas, Gareth J.

2019-06-20

Appleby-Thomas GJ, Jaansalu K, Hameed A, et al., (2019) A comparison of the ballistic behaviour of conventionally sintered and additively manufactured alumina. Defence Technology, Volume 16, Issue 2, April 2020, pp. 275-282

https://doi.org/10.1016/j.dt.2019.06.020